THE JOURNAL OF PHYSICAL CHEMISTRY B

Article

pubs.acs.org/JPCB

Multiscale Modeling of the Nanomechanics of Microtubule Protofilaments

Kelly E. Theisen,[†] Artem Zhmurov,[‡,§] Maycee E. Newberry,[†] Valeri Barsegov,[‡,§] and Ruxandra I. Dima*[,†]

[†]Department of Chemistry, University of Cincinnati, Cincinnati, Ohio 45221, United States

[‡]Department of Chemistry, University of Massachusetts, Lowell, Massachusetts 01854, United States

[§]Moscow Institute of Physics and Technology, Moscow Region, Russia, 141700

Supporting Information

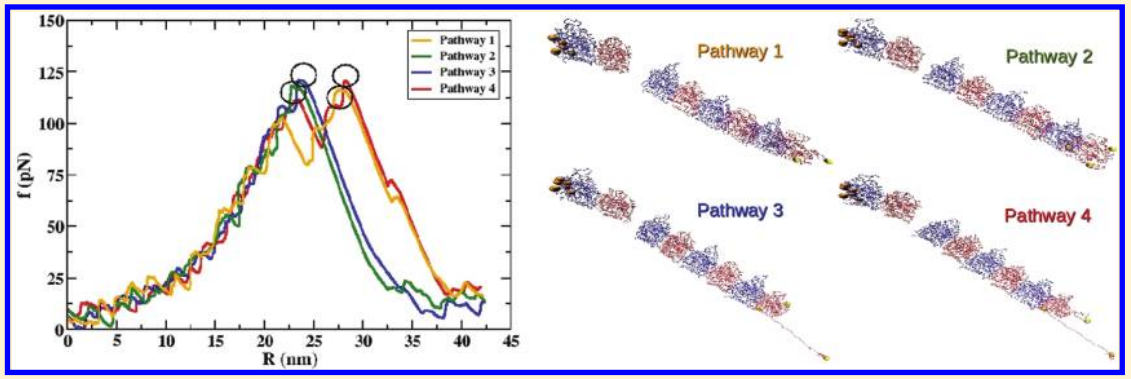

ABSTRACT: Large-size biomolecular systems that spontaneously assemble, disassemble, and self-repair by controlled inputs play fundamental roles in biology. Microtubules (MTs), which play important roles in cell adhesion and cell division, are a prime example. MTs serve as "tracks" for molecular motors, and their biomechanical functions depend on dynamic instability—a stochastic switching between periods of rapid growing and shrinking. This process is controlled by many cellular factors so that growth and shrinkage periods are correlated with the life cycle of a cell. Resolving the molecular basis for the action of these factors is of paramount importance for understanding the diverse functions of MTs. We employed a multiscale modeling approach to study the force-induced MT depolymerization by analyzing the mechanical response of a MT protofilament to external forces. We carried out self-organized polymer (SOP) model based simulations accelerated on Graphics Processing Units (GPUs). This approach enabled us to follow the mechanical behavior of the molecule on experimental time scales using experimental force loads. We resolved the structural details and determined the physical parameters that characterize the stretching and bending modes of motion of a MT protofilament. The central result is that the severing action of proteins, such as katanin and kinesin, can be understood in terms of their mechanical coupling to a protofilament. For example, the extraction of tubulin dimers from MT caps by katanin can be achieved by pushing the protofilament toward the axis of the MT cylinder, while the removal of large protofilaments curved into "ram's horn" structures by kinesin is the result of the outward bending of the protofilament. We showed that, at the molecular level, these types of deformations are due to the anisotropic, but homogeneous, micromechanical properties of MT protofilaments.

INTRODUCTION

Biomechanical functions of protein fibers including microtubules (MTs) and actin filaments, which exhibit unusual physicochemical properties such as viscoelasticity and spontaneous shape changing, are important in cytoskeletal support and cell motility. Understanding the microscopic origin of these unique properties and elucidating the molecular mechanisms of the response of biological assemblies to controlled mechanical inputs constitute major areas of research in biochemistry and biophysics. Although state-of-the-art single-molecule experiments have become available to explore these properties,[1,2] due to their high complexity (~10^3–10^5 amino acids) and large size (~50–200 nm), these experiments yield results that are nearly impossible to interpret accurately without some input from theoretical modeling.[2,3] Consequently, linking the submolecular transitions to observed changes in structural and dynamic properties at the macroscopic level has emerged as one of the main challenges of the day.

It has been long recognized that the unique features associated with the native topology, rather than atomic details, govern the mechanical properties of large-size biological

Special Issue: B: Macromolecular Systems Understood through Multiscale and Enhanced Sampling Techniques

Received: December 30, 2011
Revised: April 13, 2012
Published: April 16, 2012

   dx.doi.org/10.1021/jp212608f | J. Phys. Chem. B 2012, 116, 8545–8555

systems.[4] One of the descriptions, which emphasizes the importance of native topology, is the C_α-based self-organized polymer (SOP) model.[5] The SOP model provides a simplified yet accurate topology-based description of the polypeptide chain of proteins, which proved to be essential to describe the mechanical properties of biomolecules, including the green fluorescent protein,[6] kinesin,[7] myosin V,[8] actin,[9] synaptotagmin 1,[10] and fibrinogen[11] among many others. We performed computational exploration and theoretical modeling of the protofilaments (PFs) of MTs using SOP model based simulations accelerated on a Graphics Processing Unit (GPU). The main advantage of the SOP-GPU approach is that these simulations enable us to follow the dynamics of MTs in the experimental centisecond time scale, employing realistic force loads used in atomic force microscopy (AFM).[12,13]

MTs are made of $\alpha\beta$-tubulin heterodimers joined longitudinally into protofilaments, which then associate laterally to form a polar cylindrical structure of ∼13 protofilaments (PFs). Prior to inclusion in the MT lattice, tubulin dimers bind one guanosine 5′-triphosphate (GTP) per monomer. Upon polymerization into MTs, GTP in β-tubulin hydrolyzes, but the MT cylindrical structure is believed to be stabilized by a GTP cap consisting of a number of layers of tubulin subunits with GTP bound to both monomers.[14] MTs exhibit dynamic instability both in vivo and in vitro.[15] This defining behavior is fundamental for their function since interactions of MTs with cellular cofactors, molecular motors, and severing proteins are driven by this dynamics. The assembly and disassembly of MTs do not occur through simple helical growth or shrinkage of individual tubulin subunits but rather through a series of unstable polymeric intermediates.[15] This makes it very challenging to pinpoint the exact microscopic origin of their complex cellular behavior. During MT depolymerization, the weak lateral bonds between PFs break first, leading to so-called "ram's horns" structures, in which the PFs curl outward from the MT axis.[16] These curved structures dissociate from the MT to form circular structures of one or two stacked rings, in which the outer (inner) ring contains 16 (12) tubulin dimers.[17] Cryo-EM structures give a diameter of ∼40−42 nm for the ram's horn structures and for the interior diameter of the ring structures.[18]

MT-severing enzymes are cellular factors that are directly involved in the control of the dynamic instability by targeting individual PFs.[19] On the basis of the results of fluorescence microscopy measurements, Ross and collaborators[20] proposed that one such enzyme, katanin, interacts with the C-terminal end of β-tubulin and removes tubulin dimers from MT ends. An immediate consequence of this proposal is that there is a preference for depolymerization to start at the plus end, which implies that the rate of depolymerization from the plus end is faster than that from the minus end. Ross et al.[20] also found that katanin appears to target to PF-shift defects because uniform katanin binding along the MT was not detected even at high concentrations. Hence, the mechanism here is the removal of tubulin subunits, rather than large PF fragments, from the MT lattice. This behavior is in stark contrast with the depolymerization mechanism of kinesin, such as Kinesin-13s, which acts by peeling off PFs from the lattice.[21] Because efficient depolymerization of MTs must involve peeling off PFs, Ross et al. proposed that severing enzymes act by cutting the stabilizing end-caps to activate depolymerization by kinesins[20] such as MCAK which appears to bind better to bent PFs found at uncapped ends of MTs.[22] Spastin, an AAA ATPase which, upon ATP hydrolysis, assembles into hexameric rings, has two regions that are crucial for attachment and severing of MTs: the N-term microtubule binding domain (MTBD) region (residues 270−328) and the C-term region (residues 343−616).[23] While experiments did not resolve the region of coupling between the N-term MTBD part of spastin with the MT lattice, the C-term domain of spastin in the hexameric form was found to form contacts with the acidic C-terminal end of either α- or β-tubulin. These biochemical studies also revealed that the N-term MTBD region of interaction with MTs is different from that for the C-term region. This implies that a severing protein needs to establish bonding contacts with the MT lattice in more than one region to induce depolymerization.[19,23]

These recent studies pose a number of interesting questions. How do the intrinsic bending properties of MT PFs account for the considerably large radius of the ram's horns? Why are the ram's horns at the minus end of MTs smaller than those at the plus end?[16] What are the structural characteristics of MTs that facilitate the mode of action of severing proteins? To address these questions, we conducted large-scale simulations of the mechanical bending of MT PFs to determine molecular factors that drive depolymerization of MTs. To achieve this goal, we employed a multiscale approach to explore the mechanical behavior of MTs on multiple spatial scales from individual tubulin subdomains to full PFs. Until recently, the two main approaches used toward understanding the MT bending dynamics have been theoretical models and finite element modeling (FEM) to characterize the flexural rigidity from buckling, thermal bending, optical tweezers, or AFM experiments.[1−3,24,25] The strength of the FEM is that it helps follow the mechanical response of a large system on the micrometer scale, but it neglects the intimate molecular details of a MT. For example, the FEM analysis for tubulin dimers uses a simplifying assumption that the dimers and the PFs in a MT are homogeneous and isotropic. Molecular dynamics (MD) simulations employing atomistic models of MT protofilaments[26] and the MT cylinder[27] have been used to measure the flexibility of these systems subject to the thermal perturbation. Unfortunately, due to the very high computational cost, MD simulations are limited to the time duration of a few tens and hundreds of nanoseconds. This is shorter by many decades of biological time than the typical time scale of a few seconds or even longer, which characterizes the mechanical response of MTs.[28] Besides, these computational approaches are limited to the harmonic regime (near-equilibrium elastic deformation) and, hence, cannot be used to describe the MT depolymerization. In this respect, the SOP-GPU approach enables us to describe the nonlinear response of long PFs of MTs in the experimentally relevant time scale, without neglecting important molecular details.

The main results from our study are the following. First, bending of a PF in the outward direction from the MT cylinder axis always results in the disruption of the interdimer interface closest to the fixed subunit. This implies that the dissociation of PFs occurs through the formation of an intermediate partially depolymerized state, in accord with experimental results.[15] In contrast, bending in the interior direction (pushing) leads mostly to the fragmentation of the PF into tubulin subunits or smaller fragments of two subunits. These results enable us to provide new mechanistic insights for the action of severing proteins. If spastin and katanin act by removing tubulin units from the MT cylinder, then they perform their function primarily by pushing on the tubulin cap. Second, we found that

dx.doi.org/10.1021/jp212608f | J. Phys. Chem. B 2012, 116, 8545−8555

interior tubulin subunits behave distinctly different from subunits at the PF end. This is because the α-tubulin monomer is the weakest link in the interior dimer. In our previous studies, we found that β-tubulin was the most flexible part of the end tubulin dimer.[29] Third, the tubulin dimer shows a large mechanical anisotropy: the mechanical response of an interior dimer to an applied force changes dramatically upon a small change in the direction of applied force. This points to the fact that tubulin is capable of adapting to its cellular interactions by adjusting its mechanical response through changing the direction of interaction with partner proteins. Fourth, we found that the bending of a PF results in the breaking of tubulin dimers (or longer PF fragments) only when the mechanical force is applied simultaneously to multiple locations across the exposed surface of the end monomer. This correlates well with the proposed mechanism that MT depolymerizing proteins use multiple, spatially separated, points of attachment on the surface of a tubulin dimer.[19] Finally, we found that severing proteins cannot remove an interior dimer from a PF made of straight GDP-bound units by pulling on the C-term end of the β-tubulin. This action would have resulted in the monomer unfolding and disruption of the intradimer interface under the influence of mechanical force far exceeding the maximum ~150 pN force that AAA ATPase proteins exert.[30] Hence, taken together, our results indicate that a PF shows homogeneous, but anisotropic, mechanical properties.

METHODS

Self-Organized Polymer (SOP) Model. In our simulations, we used the SOP model, which is based on the native topology of a protein. In this model, each amino acid residue in the structure of the tubulin heterodimer (PDB entry 1TUB) or the PFs of MTs from Wells and Aksimentiev[27] is represented by its C_α atom.[5] The total potential energy function for a protein conformation, specified in terms of the coordinates $\{r_i\}$ (i = 1, 2, ..., N), where N is the total number of residues, is given by

$$\begin{aligned} V_T &= V_{FENE} + V_{NB}^{ATT} + V_{NB}^{REP} \\ &= -\sum_{i=1}^{N-1} \frac{k}{2} R_0^2 \log\left(1 - \frac{(r_{i,i+1} - r_{i,i+1}^o)^2}{R_0^2}\right) \\ &+ \sum_{i=1}^{N-3} \sum_{j=i+3}^{N} \varepsilon_h \left[\left(\frac{r_{ij}^o}{r_{ij}}\right)^{12} - 2\left(\frac{r_{ij}^o}{r_{ij}}\right)^6\right]\Delta_{ij} \\ &+ \sum_{i=1}^{N-2} \varepsilon_l \left(\frac{\sigma_{i,i+2}}{r_{i,i+2}}\right)^6 + \sum_{i=1}^{N-3} \sum_{j=i+3}^{N} \varepsilon_l \left(\frac{\sigma}{r_{ij}}\right)^6 (1 - \Delta_{ij}) \end{aligned} \quad (1)$$

where i + 1 is $r_{i,i+1}$ and $r_{i,i+1}^o$ is the corresponding value in the native structure. The first term in eq 1 is the backbone chain connectivity (FENE) potential. The second term (V_{NB}^{ATT}) accounts for the nonbonded (noncovalent) interactions that stabilize the native (folded) state. If the noncovalently linked residues i and j ($|i - j| > 2$) are within a cutoff distance R_C (i.e., $r_{ij} < R_C$ = 8 Å), then Δ_{ij} = 1 and 0 otherwise. A uniform value of ε_h = 2.0 kcal/mol, which quantifies the strength of nonbonded interactions, is assumed following our previous tubulin studies.[29,31] All the non-native interactions (V_{NB}^{REP}), described by the third and fourth terms in eq 1, are treated as repulsive. Also, in eq 1, R_0 = 2 Å and ε_l = 1 kcal/mol.

MT Simulation Details. We carried out Langevin simulations for all the systems at room temperature (T = 300 K). The integration time step h was computed as $h = 0.16\tau_H$, where $\tau_H = \zeta\varepsilon_h\tau_L/k_BT$ is the characteristic time for Brownian motion.[32] Here, ζ = 50—the dimensionless friction coefficient—accounts for the high friction regime (overdamped limit); τ_L is the time scale for Langevin dynamics; and k_BT is the thermal energy (k_BT = 0.6 kcal/mol at T = 300 K). For tubulin in the high friction regime, τ_L is 2 ps,[5,29,32] which leads to the integration time step h = 53 ps. To mimic the experimental force-ramp measurements, we applied the time-dependent pulling force $f(t) = k_s v_f t$ to selected positions for each system (tagged residues) moving them with the constant pulling speed (v_f) in the direction of the vector connecting the tagged residues with the constrained residues (simulations of stretching) or in the direction perpendicular to the main axis of the protofilament (simulations of bending) while keeping the constrained residues fixed. The list of tagged residues, which is based on the set of interdimer contacts between tubulin subunits in MTs identified by Nogales et al.,[33] is provided in Table S1 in the Supporting Information (SI). The cantilever spring constants of k_s = 17.5 pN/nm for PFs and 35 pN/nm for the tubulin dimer are within the experimental ~10−100 pN/nm range used in AFM. We set the pulling speed to v_f = 1.9 μm/s. In the simulations for the tubulin dimer, we stretched the dimer by applying force to one position in the β-tubulin monomer while keeping one position in the α-tubulin monomer fixed. In the PF studies, we used a PF dimer (two tubulin dimers joined longitudinally) and tetramer (four tubulin dimers joined longitudinally), both in the straight (GTP-like) conformation. The simulation setup for bending studies is presented in Figure 1 and Figure S1 in the SI. The idea is to apply a bending force to positions at the terminal plus-end in the β-tubulin monomer, while keeping selected positions in the α-tubulin monomer at the minus end constrained (plus-end bending). For bending at the minus-end of the filament, the force was applied to a set of positions in the α-tubulin monomer at the minus-end, while keeping selected positions at the terminal plus-end in the β-tubulin monomer fixed. The details of pulling simulations are summarized in Table S2 in the SI. To describe the intradimer interfaces, when tubulin subunits are part of the PF structure, we used the Full-Go (FG) SOP model introduced in our recent

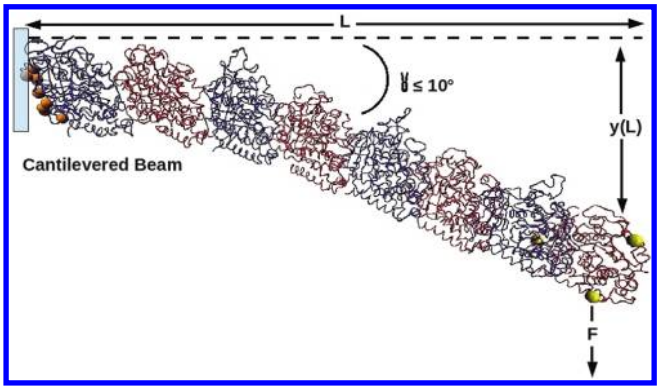

Figure 1. Schematic of the cantilevered beam system in which one end of a flexible rod is fixed, while force is applied at the opposite end to induce bending. We used it as a model for the bending of MT PFs that allows us to extract various mechanical parameters from the simulations as described in the Methods.

dx.doi.org/10.1021/jp212608f | J. Phys. Chem. B 2012, 116, 8545−8555

study of synaptotagmin 1[10] (see Section 1 in the SI for details). For computational speed-up, we performed the simulations using the GPU implementation of the SOP model (SOP-GPU package).[12,13]

MT Data Analysis. The values of the critical force and molecular elongation were taken from the simulated curves of the mechanical response (force) versus molecular extension, called the force−extension curves (FECs). To analyze the results of pulling and bending simulations, we used a number of parameters that characterize the mechanical response of a PF. These are the Young's modulus E, a measure of the elasticity of the PF, calculated from stretching simulations; the bending angle θ formed by the intrinsic coordinates of the PF and the critical bending angle γ compared to the starting orientation of the PF (reference state) depicted in Figure 1 and Figure S2 in the SI; the flexural rigidity parameter EI in the linear approximation (bending simulations); and the persistence length L_p. For the Young's modulus, we used the standard equation $F/A = E\Delta L/L$, where F is the force applied to stretch a PF; $A = 1.66 \times 10^{-17}$ m^2 is the cross-sectional area of a PF; and $\Delta L/L$ is the strain, i.e., the ratio of the molecular extension ΔL to the initial length of the molecule L. This relationship holds in the elastic regime up to $\Delta L/L \approx 0.025$ strain.[27] Next, we used the values of E to determine EI based on the second moment of inertia (I) for a slender rod with circular cross-section, $I = \pi r^4/4 = 2.20 \times 10^{-35}$ m^4. For the bending motion, we calculated EI as EI $= FL^3/3y(L)$, which is the solution of the small-angle beam equation for a rod clamped at one end (the cantilevered beam depicted in Figure 1). At the same time, the persistence length L_p is given by $L_p = \mathrm{EI}/k_BT$. For the PF tetramer, $L = 34$ nm is the initial length. The values of $y(L)$ were obtained using the difference between the PDB coordinates of one of the pulled residues in the reference state and in the transient structure (see Table S3 in the SI for pulled residues). We also determined the elastic spring constant for the bending of a PF, κ, treated as a cantilevered beam (Figure 1) using the formula $\kappa = 3\mathrm{EI}/L^3$. The bending angles θ and γ correspond to the dot products of the two vectors connecting the center of mass (COM) of each chain in the structure analyzed (see Figure S2 in the SI). More information on the mechanical properties referenced here can be found in ref 23.[28]

RESULTS

Stretching of Interior Tubulin Dimers in the MT Lattice Shows Anisotropy. We probed the molecular basis of the dynamic behavior of MT protofilaments by following the mechanical response of an interior tubulin subunit to an external force. This part of the study and our previous results[29,31] allowed us to resolve the micromechanics of the individual subunits in isolation and helped us compare their physical properties with their properties in the full PF. We followed the response of a tubulin dimer to an external load along three different directions of pulling force (listed in Table S1 in SI) relevant for the interior units[33] and under regimes of varying force. Testing the system for different geometries of force application was inspired by AFM studies, which showed that a change in the pulling direction affects not only the unfolding pathway but also the critical unfolding force.[34] A detailed description of our results, together with the corresponding figures and tables, is presented in Section 2 in the SI. Our central finding is that the tubulin dimer is highly anisotropic (see Table S4 and Figures S3 and S4 in the SI for details). Indeed, varying positions/directions of force application result in different unfolding scenarios and critical forces. These are different from our results for the end units.[29] This important finding correlates well with the recent work of de Pablo et al.,[35] where it was found that changing the orientation of the cantilever tip relative to the MT affects the magnitude and duration of the force signal.

Stretching of Protofilaments Results in the Release of the Terminal Unit. We applied a pulling force to the PF dimer and tetramer. For both systems, we observed a single depolymerization pathway characterized by the disruption of the interdimer interface closest to the pulled position, while no monomer unfolding was detected (Figure S5 in the SI). The critical force ranged from 450 to 480 pN at an 8 nm extension, which corresponds to the dimer size. We calculated the Young's modulus for the PF by determining the force experienced by the molecule at a strain of 0.025 (2.5% extension) which, according to Wells and Aksimentiev,[27] corresponds to the harmonic regime of molecular elongation. We obtained 0.382 GPa for the tetramer under a force of 159 pN (see Table 1), which agrees well with the results of all-atom simulations.[27] Hence, the results obtained validate the use of the coarse-grained description of the tubulin subunits. The experimental range is 0.2−1.9 GPa,[28] but the experimental and simulated results cannot be compared since the experimental values correspond to an entire MT, not a single PF.

Table 1. Mechanical Characteristics of Microtubule Protofilaments Obtained from Simulations of Force-Induced Stretching: The Critical Force, Young'S Modulus (E), Flexural Rigidity EI, and Persistence Length L_p

system	force (pN)	E (GPa)	EI (N m^2)	L_p (μm)
2 dimer protofilament	124	0.299	6.57×10^{-27}	1.60
4 dimer protofilament	159	0.382	8.40×10^{-27}	2.05

Bending at the Plus End of a Protofilament. It is known that the majority of MT severing proteins and microtubule-associated proteins (MAPs) target the plus end of the MT cylinder, more specifically, the acidic C-term end of β-tubulin at the plus end. As mentioned in the Introduction, in general MT polymerization and depolymerization occur more rapidly at the plus end, and depolymerization proceeds through formation of intermediate states, characterized by the removal of the GTP cap and the outward bending of PFs. Moreover, the size of the bent PFs (ram's horns) at the plus end exceeds that of the bent PFs at the opposite end. To shed light on the origin of these transitions, we examined the bending behavior of the plus end portion of a single PF. Recent MD simulations of a fragment of a PF trimer (three dimers joined longitudinally) revealed that, irrespective of the initial state, the PF experiences thermal bending with equal probability both in the interior and outward directions.[26] For this reason, we investigated the behavior of the fragment of a PF tetramer by applying bending forces in the interior direction (toward the axis of the MT cylinder) and in the outward direction (away from the axis of the cylinder), which we denote the C-term direction. A summary of the breaking forces and the critical bending angles is presented in Table 2.

A. Interior Bending Results in the Fragmentation of the Protofilament. We found four distinct pathways of bending of the PF in the interior direction and no preference of the system for detachment at a particular interdimer interface (Figure 2).

dx.doi.org/10.1021/jp212608f | J. Phys. Chem. B 2012, 116, 8545−8555

Table 2. Summary of the Results from Simulations of PF Bending[a]

system	pathway	interface	average force (pN)	θ	γ
Bending from Plus End:					
interior (pulling 3 resid.)	1 (30%)	central dimer	149 ± 1	16°	47°
	2 (30%)	fixed dimer	141 ± 5	15°	48°
	3 (10%)	pulled dimer	118	20°	45°
	4 (30%)	pulled dimer	140 ± 4	14°	44°
C-term (pulling 3 resid.)	1 (30%)	fixed dimer	122 ± 3	12°	44°
	2 (30%)	fixed dimer	115 ± 6	14°	43°
	3 (10%)	fixed dimer	118 ± 4	12°	45°
	4 (30%)	fixed dimer	123 ± 2	15°	48°
Bending from Minus End:					
tnterior (pulling 3 resid.)	1 (85%)	pulled dimer	127 ± 6	16°	41°
	2 (15%)	central dimer	125 ± 1	16°	42°
C-term (pulling 3 resid.)	1 (90%)	pulled dimer	124 ± 4	15°	44°
	2 (10%)	fixed dimer	120	12°	44°

[a]For each pulling setup, we list the pathways, pathway probabilities, the interface at which the force-driven dissociation occurs, the average critical force (with standard deviation), and the critical angles θ and γ. The pulled residues are listed in Table S1 from the SI.

Pathway 1 (observed 30% of the time) showed unfolding of residues 70 to 99 and 386 to 420 at the N-terminal and C-terminal domains of the pulled β-tubulin monomer, which was followed by the disruption of the central interdimer interface. In Pathway 2 (30%), the same regions in the β-tubulin have unfolded, but the interdimer interface closest to the fixed positions has disrupted. In contrast, Pathways 3 (10%) and 4 (30%) showed opening of the interdimer interface closest to the pulled positions. While no unfolding was detected for Pathway 3, residues 70 to 99 in the pulled β-tubulin monomer unfolded in Pathway 4 prior to the interface opening. The critical force was approximately 125 pN (acting on each pulled residue) for all four pathways. Although these pathways characterize the behavior of one PF, they are unlikely to be observed for the entire MT cylinder due to the molecular extension required for the detachment of subunits. Indeed, because the inner diameter of MT is ∼18 nm, then within ∼15 nm of bending extension the PF would experience repulsive interactions with the opposite MT wall. Hence, Pathways 1 and 2 (which correspond to the detachment of 2 or 3 dimers) are unlikely to occur. Pathways 3 and 4, which correspond to the detachment of only one tubulin dimer from the plus end of the PF, represent plausible depolymerization scenarios even for the full MT cylinder since the presence of lateral bonds between a PF and its two nearest neighbors is expected to result in a reduced bending distance.

B. Outward (C-Term) Bending Results in the Detachment of a Large PF Fragment. Bending of a PF in the outward direction under mechanical forces acting on spatially separated

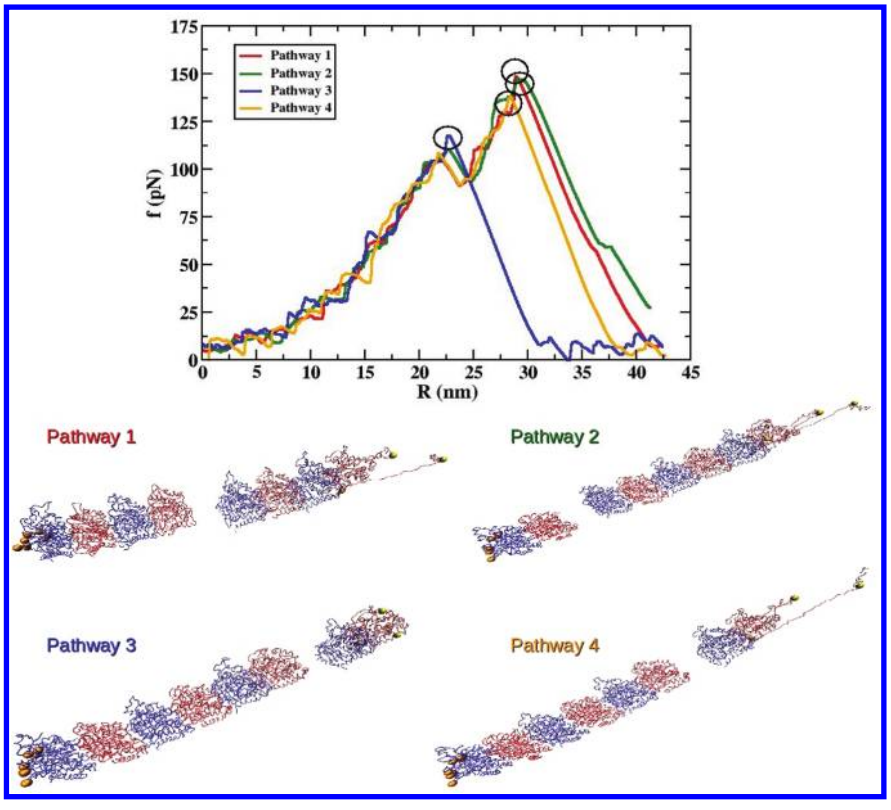

Figure 2. Bending the MT PF in the interior direction. Force setup: pulling three residues in the β-tubulin monomer at the plus end of the PF (see Methods and Table S1 in the SI). Shown are the force (f)−extension (R) curves for the four pathways detected. Conformational snapshots corresponding to the onset of PF depolymerization (encircled force peaks in FECs) for each pathway are displayed on the bottom. These snapshots show that bending of the MT PF in the interior direction leads to the fragmentation of the PF. We used the VMD and PovRay packages[48] for visualization.

dx.doi.org/10.1021/jp212608f | J. Phys. Chem. B 2012, 116, 8545−8555

positions in the terminal β monomer yielded four distinct pathways. In contrast to the results for the interior bending, these pathways only differed in terms of the extent of unfolding at the plus end in the β-tubulin monomer prior to detachment, as they all showed disruption of the interdimer interface closest to the fixed positions. Thus, in this case, three dimers dissociated together in all the pathways. Pathway 1 (30%) revealed unfolding of residues 70−99 from at the N-terminal domain in the β-tubulin. In Pathway 2 (30%), no unfolding was detected. In Pathway 3 (10%), residues 385 to 420 in the C-terminal domain unfolded. Finally, Pathway 4 (30%) showed the mixed unfolding detected in Pathways 1 and 3 (see Figure 3). Similarly to the interior bending, we found that the critical force experienced by the pulled positions was ∼125 pN.

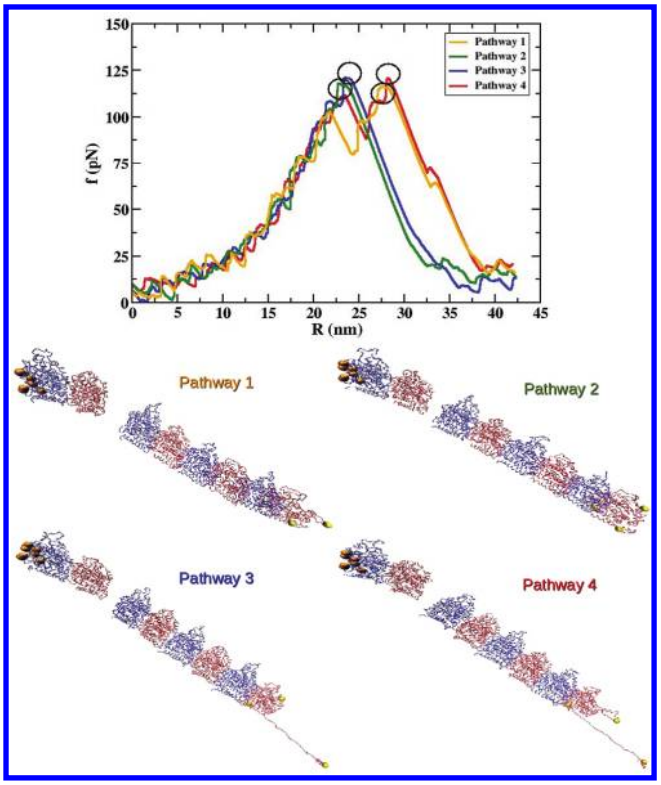

Figure 3. Bending the MT PF in the C-term direction at the plus end. Force setup: pulling three residues in the β-tubulin monomer at the plus end of the PF (see Methods and Table S1 in the SI). Shown are the force−extension curves for the four pathways detected. Structural snapshots corresponding to the onset of PF depolymerization (encircled force peaks in FECs) for each pathway are displayed on the bottom. These configurations indicate that in all pathways the interdimer interface that breaks is the one closest to the fixed positions (orange spheres) at the minus end of the PF.

To resolve the dynamics of tension propagation, which results in the PF bending and dissociation, we followed the temporal evolution of the backbone contacts at the various domain interfaces across the PF structure. The results are summarized in Table S5 in the SI. The distribution of the total number of interdimer contacts broken at each interface was similar in all four pathways. This indicates that tension propagates uniformly in the PF and that there is no bias in favor of the HC interface (closest to the fixed positions) where the largest amount of contacts disrupt. For example, in Pathway 1 when a part of the HC interface disrupted at 12 ms, we observed breakage of 23 contacts (out of 51). The same number of contacts broke in the AD interface (middle) at 16.4 ms in Pathway 2. For the BE interface near the pulled monomer, the same amount of contacts broke in Pathway 3 at 17.4 ms (third step). Analysis of broken contacts across the interdimer interface for Pathway 2 (Figure 4) showed that the contacts broken at each step are uniformly distributed. In contrast, the intradimer backbone contacts broken in Pathways 2 and 3 (Table S6 in SI), displayed in Figure 4, were localized in the inner MT surface. In addition, the percentage of intradimer contacts broken was negligible compared to the interdimer contacts, which was expected given the large stability of the dimer to denaturation.

The MT severing protein katanin was proposed to bind exclusively to the C-terminal residue of tubulin (the α monomer at the minus end and the β monomer at the plus end). To test this hypothesis, we carried out bending simulations by fixing the same set of positions as described above, while pulling only the C-terminal residue in the β tubulin monomer at the plus end of the PF. We detected only two bending pathways, which occurred with equal probability (Figure S6 in the SI). In Pathway 1, characterized by a critical force of 440 pN, the C-terminal domain and a part of the middle domain in the pulled β-tubulin (residues 210 to 420) unfolded. This was followed by the disruption of the intradimer interface linking the pulled β monomer and the corresponding α-tubulin monomer. In contrast, Pathway 2 (critical force of 390 pN) showed unfolding of residues 388 to 420 from the β-tubulin monomer, which occurred prior to the opening of the interdimer interface closest to the fixed positions. This pathway is similar to Pathway 3 discussed above.

Bending at the Minus End of a Protofilament. While the plus end of a MT cylinder is the primary attachment location for most MAPs, polymerization and depolymerization of the MT lattice also occur at the minus end. For example, laser optical tweezers experiments found that MCAK depolymerizes the minus end of a MT three times faster than its plus end at a rate of 3.3 nm s^{-1} but under a higher critical force.[22] To compare the mechanical responses from the two ends of a MT and determine the degree of homogeneity of the structure, we conducted PF tetramer bending studies under applied mechanical forces to selected positions in the α-tubulin monomer located at the minus end (see Methods and Table S1 in the SI for details).

A. Interior Bending at the Minus End Leads to Protofilament Fragmentation. We found two pathways for the bending of the PF in the interior direction at the minus end, as depicted in Figure S7 from the SI. Both pathways start with the unfolding of positions 323 to 349 (H10) in the middle domain of the pulled α monomer followed by the breaking of an interdimer interface. This results in the formation of only one peak in the FEC (see Figure S7 in the SI). In the major Pathway 1 (85%), the mechanical unfolding was followed by the opening of the interdimer interface closest to the pulled positions. In the minor Pathway 2 (15%), the interdimer interface in the middle of the PF had disrupted. This shows that, similar to the interior bending at the plus end, the major pathway results in the removal of a single dimer, consistent with a pushing mechanism for katanin.

B. C-Term Bending at the Minus End Leads to Protofilament Fragmentation. Similarly to the interior bending, the bending motion resulting from pulling three residues at the minus end in the C-term direction showed two distinct

dx.doi.org/10.1021/jp212608f | J. Phys. Chem. B 2012, 116, 8545−8555

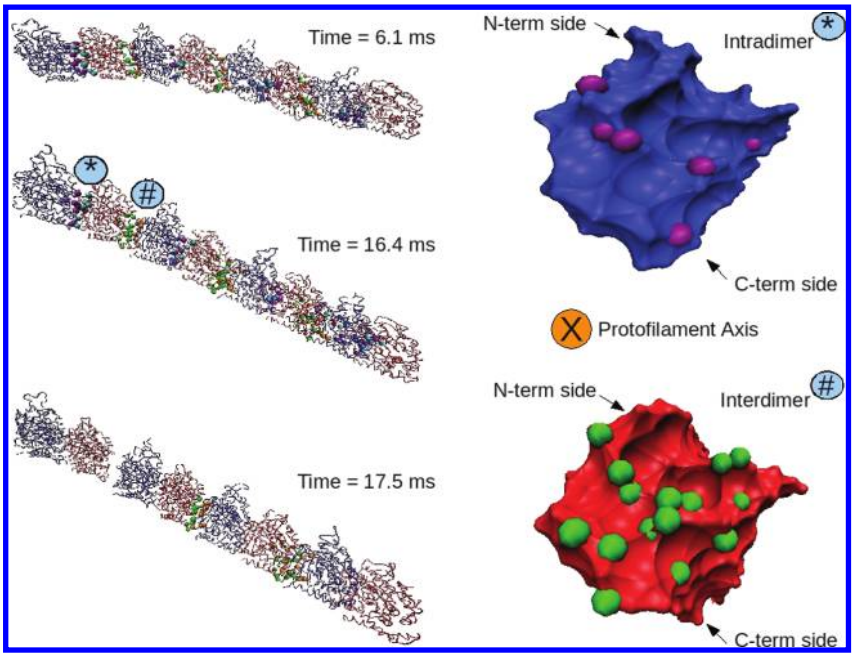

Figure 4. Diagram of the contacts broken in the two main steps in Pathway 2, obtained from bending simulations in the C-term direction at the plus end (see Figure 3). The conformational snapshots (structures on the left) correspond to the transition states (force peaks in FECs) shown in Figure 3. Here, broken contacts are represented by the colored beads: magenta beads are positions in the α-tubulin part of the intradimer interface; cyan beads are residues in the β-tubulin part of the same interface; green beads are positions in the β-tubulin part of the interdimer interface; and orange beads are residues in the α-tubulin part of the same interface. Structures on the right, shown in surface mode, represent a transient conformation of the α-tubulin monomer at the (constrained) minus end of the protofilament (upper structure) and a conformation of the β-tubulin monomer from the same dimer (lower structure), observed at time 16.4 ms. The location of each monomer in the protofilament is denoted by * and #, respectively. This representation helps locate broken contacts on the surface of each monomer in the intradimer and interdimer interface.

pathways (Figure 5). The dominant pathway is the same as Pathway 1 from above (now with 90% frequency). In the second pathway (10%), the unfolding of the H10 region of the α monomer is followed by the disruption of the interdimer interface closest to the fixed positions. The prevalence of Pathway 1 is in stark contrast with the results for the outward bending at the plus end, where we observed the opening of the interdimer interface closest to the fixed positions. Nevertheless, the critical force required to disrupt the interface (~125 pN) was unchanged. We also conducted simulations of the PF bending, in which we applied the mechanical force only to the C-term end in the α-tubulin monomer at the minus end. Here, we found only one pathway, in which we observed partial unfolding of a large fragment of the α monomer (at ~150 pN force), which occurred prior to the opening of the intradimer interface (at ~250 pN force) connecting it with the β monomer (Figure S8 in the SI).

We monitored the number of interdimer contacts broken during the bending of the PF from the minus end. Because Pathway 1 (disruption of the HC interface) was observed 90% of the time, we analyzed the list of broken contacts for this pathway. The results (Table S7 in the SI) were similar to those for the contacts broken at the plus end (Table S5 in the SI), which provides additional evidence for the notion that tension propagates uniformly across the protofilament structure. We analyzed the interdimer contacts for the various pathways for the outward bending at the plus and minus ends of the PF. We found that the backbone contacts broken in the main bending transitions correspond to pairs of residues that belong to the same regions: H8 (in α monomer) to the T3 and T5 loops, and H11 (in β monomer); S8 (in α monomer) to the T5 loop (in β monomer); H10 (in α monomer) to the T5 loop, H6, and H7

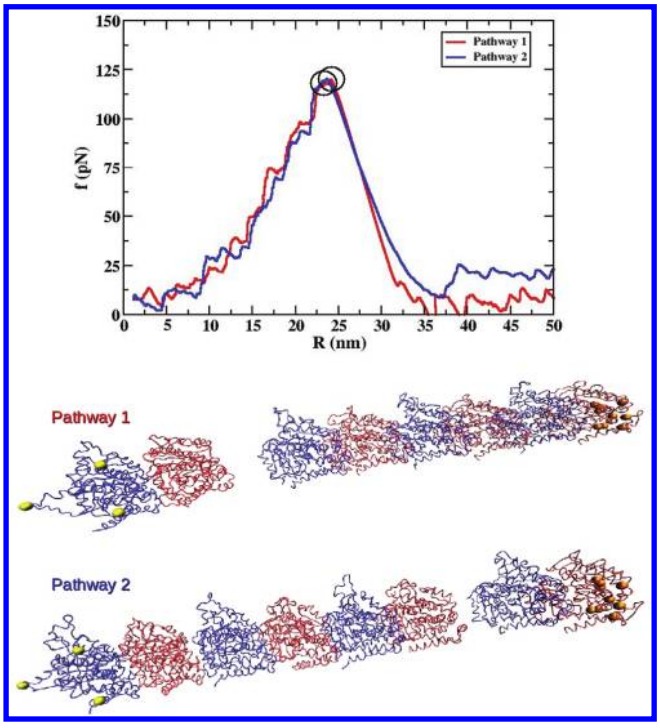

Figure 5. Bending the MT PF in the C-term direction at the minus end. Force setup: pulling three residues in the α-tubulin monomer at the minus end of the PF (see Methods and Table S1 in the SI). Displayed are the force–extension curves for the two pathways detected. Transition state structures corresponding to the onset of PF depolymerization (encircled force peaks in FECs) for each pathway are displayed on the bottom.

dx.doi.org/10.1021/jp212608f | J. Phys. Chem. B 2012, 116, 8545–8555

(in β monomer); and S9 (in α monomer) to the T5 loop and H11 (in β monomer). That similar contacts broke upon bending the PF in the C-term (outward) direction from either end indicated that the PF remains homogeneous under bending tension. For bending at the plus end, analysis of contacts reveals that the broken intradimer contacts were localized to the following regions: T3 (in α monomer) to S4 and S8 (in β monomer); T5 (in α monomer) to S9 (in β monomer); H7 (in α monomer) to H10 and T7 loop (in β monomer); and H11 (in α monomer) to T7 loop, H8, and S9 (in β monomer). These regions are different from those reported in our studies for the end tubulin dimers.[31] These result are expected in view of tubulin anisotropy and of the different geometries of force application. However, our results strongly indicate that an isolated tubulin dimer behaves differently compared to the tubulin dimer when part of the PF.

We extracted the physical parameters, which characterize the mechanical properties of a MT protofilament (see Methods). These parameters are listed in Table 2 and Table 3. We found

Table 3. Mechanical Characteristics of the PFs Obtained from the Simulations of Force-Induced Bending: The Flexural Rigidity EI, Persistence Length L_p, and Elastic Spring Constant κ

system	EI (Nm^2)	L_p (μm)	κ (pN/nm)
Bending from Plus End:			
interior (pulling 3 resid.)	7.97×10^{-26}	19.44	2.02
C-term (pulling 3 resid.)	8.07×10^{-26}	11.81	2.04
C-term (pulling 1 resid.)	7.42×10^{-26}	10.86	1.88
Bending from Minus End:			
interior (pulling 3 resid.)	13.39×10^{-26}	19.59	3.39
C-term (pulling 3 resid.)	10.44×10^{-26}	15.28	2.64
C-term (pulling 1 resid.)	5.72×10^{-26}	8.37	1.45

that the bending angle θ (for the pathways listed in Table 2) exceeds the upper limit (10°) from the distribution for bending angles for straight PFs obtained from all-atom MD simulations.[26] This is not unexpected since in our simulations the bending force substantially exceeded the thermal force, which allowed us to probe the PF bending beyond the linear regime. Moreover, for all the bending geometries corresponding to multiple points of application of force, the outward bending angle, γ, is always ~40° (Table 3). In plants, this is the exact angle at which cortical MTs nucleate off the wall of a pre-existing MT.[19] Given that katanin releases the new MTs from the branch point,[19] the agreement between our value for γ and the experimental one lends additional support that our studies reveal mechanistic insights into the mode of action of AAA ATPase severing proteins. Interestingly, the obtained EI value of $\sim 8.84 \times 10^{-26}$ Nm^2 was very close to the experimental value for an actin filament (7.3×10^{-26} Nm^2),[24] which is the likely counterpart of a MT protofilament. The calculated persistence length $L_p \approx 14$ μm was close to the measured value of 17.7 μm for an actin filament.[24] On the basis of these results, we hypothesize that the difference of 2 orders of magnitude between our EI value and the experimental value for the full MT cylinder (7.9×10^{-24} Nm^2)[36] is due to the contribution of the lateral bonds that connect the PFs in the cylinder. Both EI and L_p from the bending simulations were 1 order of magnitude higher than the values of the same quantities obtained from the PF stretching simulations (see Table 1). This is a clear signature of the mechanical anisotropy of the filament. Recent studies reported anisotropy only for full MTs due to the shearing of PFs.[3,36] However, our results show that the anisotropy is already manifest at the level of protofilaments. This implies that corrections in the interpretation of experimental MT bending data are needed to account for the additional source of mechanical anisotropy.

Outward Pulling of Interior Dimer Mimics Katanin's Action on MT Lattice Defects. Ross and collaborators recently proposed[20] that katanin, a major MT severing protein, does not bind uniformly along a MT cylinder, but rather it targets the MT caps and lattice defects corresponding to bent dimers. To provide insight into the molecular basis of this action, we set out to determine the critical force and mechanism for the extraction of an interior dimer from a straight PF. We constrained the plus and minus end portions of the PF and applied a pulling force to the C-terminal position in the β monomer of one of the two interior dimers. We found that depolymerization of the PF at the intradimer interface occurred with low probability (10%) and that the interdimer interface adjacent to the pulled monomer was disrupted most of the time (90%; see Figure 6). The corresponding 370−430 pN breaking force far exceeds the maximum force produced by katanin (~150 pN). However, the initial step is the unfolding in the C-terminal domain in the β-tubulin at ~100 pN force, which is very close to the maximal force produced by an AAA+ protein such as katanin (~150 pN).[30] Hence, our results lend support to the proposed mechanism that katanin interacts with the end-caps of a MT lattice or interior lattice defects (bent structures).

DISCUSSION AND CONCLUSIONS

We performed in-depth computational studies of the nanomechanics of microtubule protofilaments from small subunits (8 nm) to long protofilaments (34 nm) using a coarse-grained description of the polypeptide chain of proteins, the SOP model, and biomolecular simulations accelerated on GPUs. The SOP-GPU modeling enabled us to examine the dynamic behavior of MT protofilaments on time scales of tens of milliseconds. For each simulation run, the amount of the computational time is ~200 GPU-hours on a graphics card GeForce GTX 480 (from Nvidia). These long simulations have enabled us to go beyond the linear regime of reversible deformation, accessed by finite element analysis, and to obtain a number of interesting new results regarding the micromechanics of MT protofilaments. In what follows, we review and critically discuss the main results.

First, we found that bending in the C-term direction always results in the opening of the interdimer interface farthest away from the tagged region of the molecule. This finding correlates well with the existence of ram's horn structures at the plus end of the molecule[15,16] in that long curved structures do not emerge when only one or two dimers have detached at once. In contrast, force-induced bending (i.e., when force is applied to positions in the α-tubulin monomer at the minus end of the PF) almost always results in the detachment of the dimer closest to the pulled surface. This finding provides additional support for the hypothesis, which was originally formulated based on the cryo-EM data that the ram's horns at the minus end of the PF form infrequently and that they are smaller than the ram's horns formed at the opposite plus end.[16] Nevertheless, formation of these structures at either end of the filament is supported by the fact that a tubulin homologue, FtsZ, shows curvature at both ends of the filaments.[18,37]

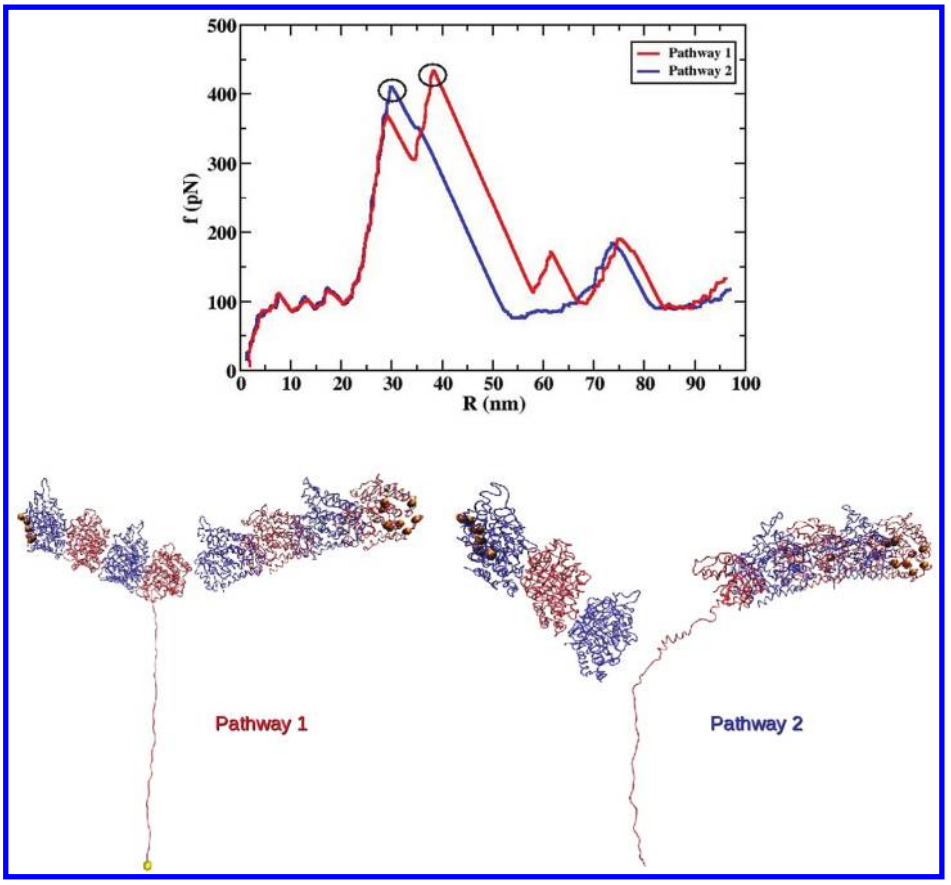

Figure 6. Simulation results for katanin-like pulling of the interior dimer in a MT PF. Force setup: constraining nine positions at the plus and minus ends of the molecule and pulling the C-terminal residue of the β monomer from one interior dimer (see Table S1 in the SI). Presented are the force−extension profiles for the two pathways detected. Structures on the bottom represent the disruption of the interface at a critical force (encircled force peaks in FECs) for each pathway. This bending setup is not physiologically relevant since Pathway 2 leads to the disruption of the intradimer interface.[38]

Mechanical bending deformation where the force is applied to only one position at the plus end of the PF is not sufficient for the emergence of the ram's horns. Indeed, this would result in the disruption of the most distant interdimer interface only 50% of the time and, most importantly, would require a large 438 pN force. At the minus end, this would never lead to the detachment of the dimer farthest away from the pulled surface. The main result of this action (i.e., 50% of the time when the pulling force is applied at the plus end and 100% of the time when the force is applied at the minus end) is the separation of the dimer into monomers, which is an unlikley event given that the measured rate of dissociation of the tubulin dimer is very low (10^{-11} M).[38]

Second, our findings regarding the bending of PFs at the plus end in the outward direction shed light on the action of kinesin as a MT depolymerizing factor. We remind that recent experiments showed that the kinesin heads bind to a single PF, 8 nm apart from each other.[35] Recent work on pKinI, a nonmotile kinesin, revealed binding at the center of each dimer, in which the relay helix of kinesin interacts with the intradimer interface leading to distortions along the PF.[21] The argument in favor of the depolymerizing action of kinesin as a promoter of formation of ram's horns structures is based on the experimental finding of the motor heads of kinesin on the inside of PF ring structures formed during depolymerization.[21] These rings have roughly the same diameter (20 nm) as those observed in vivo.[17,18,21] We found that the application of a bending force to multiple spatially separated positions at the plus end of the PF always results in considerable bending of the PF and subsequent detachment of the entire segment of dimers from the PF. This finding suggests that kinesin, which has multiple attachment points on the surface of a PF, is capable of depolymerizing the MT through an intermediate resembling the ram's horns geometry.

Third, severing proteins act on MTs in a number of cellular processes. For example, in plants katanin is involved in the release of MTs nucleated from branch points, while in *Chlamydomonas* it severs doublet MTs in the flagellum during deflagellation.[20] In mitosis of *Drosophila* S2 cells, katanin, which is localized to kinetochores and chromosomes, is required for the depolymerization of chromosome-attached MT plus ends during anaphase A. At the same time, spastin localizes to the centrosome where it is required for MT minus end depolymerization.[19] In differentiated neurons, katanin and spastin regulate axonal outgrowth and branching,[20,23] with loss of spastin function resulting in defects of dendritic arbor outgrowth.[19] Our results from the bending studies allow us to propose a mechanism for the action of MT severing proteins at the ends of MT cylinders. Experimental studies suggest that these proteins remove a single dimer at a time, as the depolymerized ends remain blunt, and do not form the ram's horn structures observed during the depolymerization of larger oligomers.[20] Our own results indicate that each severing protein needs to attach to the MT ends through multiple

dx.doi.org/10.1021/jp212608f | J. Phys. Chem. B 2012, 116, 8545−8555

binding sites, in accord with experiments.[23,39,40] Some of the attachment points have been determined experimentally.[20,23] These are the acidic C-terminal tail in the β-tubulin (α-tubulin) monomer at the plus (minus). Our results suggest that additional points of attachment could be positions 88 and 338 in the β-tubulin or in the α-tubulin. This conclusion is supported by the fact that these positions are 40−50 Å apart, which is compatible with the distance between positions in two or three adjacent monomers in the hexameric katanin. The size of katanin monomers, approximated based on a cryo-EM study of another AAA+ (p97), is 70 Å.[40] Upon firm attachment to the MT lattice, the pore loops of the severing protein exert mechanical tension on the C-terminal tail of the tubulin monomer, which is then threaded through the hexameric ring channel.[23,41,42] This generates an equal amount of pushing force to the remaining attachment points on the PF[41] which, as it follows from our simulations for interior bending, can lead to the detachment of the end tubulin dimer at the MT plus end-cap. This, in turn, might trigger partial unfolding of the target β-tubulin monomer. Our envisioned mechanism lends strong support to the recent experimentally based proposal that spastin and katanin may not need to perform a complete translacation of the tubulin chain, but rather just exert multiple tugs on the dimer to extract it from the MT lattice.[19]

Fourth, since tubulin dimers that have been removed from MTs by katanin are capable of repolymerizing back into the MT,[43] it is unlikely that complete unfolding of tubulin occurs upon severing by katanin. Because tubulin needs help from chaperones to fold properly,[44] it does not seem plausible that it would be incorporated back into the MT lattice after extensive unfolding has occurred during severing. Hence, our results from simulations for interior bending correlate well with the known depolymerization/polymerization behavior of MTs. Our results indicate that the force acting on each of the attachment points to extract the dimer by pushing on the PF is about 120−140 pN. This estimate is similar to the maximal force exterted by AAA ATPases (150 pN).[30] Katanin has also been implicated in the detachment of the minus end of MTs from the centrosome.[39,45] Our simulation data for the bending at the minus end of the PF, which showed that the removal of a single dimer was ∼90% efficient, correlate well with this function of katanin. Unlike the removal of a dimer from the plus end, where the normal force born as a reaction to an applied pushing force on the PF favors the detachment, the removal of dimers at the minus end requires a pulling force of ∼120 pN applied to all the attachment points simultaneously. This time, the normal force does not favor the detachment of a dimer, and thus, it is highly likely that the removal of dimers from the minus end would be a slow process before the pulling force reaches the optimal value. This is in accord with the observed slower rate of depolymerization by katanin at the minus end (0.047 ± 0.012 nm/s) compared to the rate for the plus end (0.092 ± 0.022 nm/s).[20]

To conclude, we have provided a mechanistic interpretation for the action of severing proteins. Also, it has long been postulated that hydrolysis of GTP at the plus end terminal in the β-tubulin monomers results in the loss of the MT cap, which triggers the catastrophe—the rapid depolymerization phase. What is not known is how many dimers deep this cap structure is. Several groups[14,46,47] have suggested that the cap size is small, only 1−4 dimers deep. Our results support this notion. We detected the physiologically relevant bending with as few as four dimers in a PF. Thus, it seems highly likely that the short fragment of only a few dimers can serve as a "nucleation point" for the ring formation and depolymerization, which whould then propagate to the dimers in the more interior region.

■ ASSOCIATED CONTENT

Supporting Information

Additional details of simulations are presented. Results for the mechanical unfolding of the interior tubulin dimer are included along with supporting figures and table. Tables summarizing the simulation protocols, the number of simulation runs, and the time evolution of the contacts at the various domain interfaces in the PF fragment of four dimers upon bending are included. Diagrams describing the simulation setups for PF bending and for the calculation of bending angles are also included. Figures describing the most typical force−extension curves and snapshots of transient conformations, which correspond to the stretching and bending of the PF fragment of four dimers, are also included. This material is available free of charge via the Internet at http://pubs.acs.org.

■ AUTHOR INFORMATION

Corresponding Author

*E-mail: ruxandra.dima@uc.edu. Phone: +1 513 5563961. Fax: +1 513 5569239.

Notes

The authors declare no competing financial interest.

■ ACKNOWLEDGMENTS

We thank Ms. Neha J. Desai from the Dima group for her help with the analysis of the time evolution of contacts at the PF interfaces. This project has been supported in part by the National Science Foundation grant MCB-0845002 (to RID) and by the Russian Ministry of Education and Science grant 02-740-11-5126 (to VB).

■ REFERENCES

(1) Schaap, I.; Carrasco, C.; de Pablo, P.; MacKintosh, F.; Schmidt, C. *Biophys. J.* **2006**, *91*, 1521−1531.
(2) Donhauser, Z.; Jobs, W.; Binka, E. *Biophys. J.* **2010**, *99*, 1668−1675.
(3) Kasas, S.; Kis, A.; Riederer, B.; Forro, L.; Dietler, G.; Catsicas, S. *ChemPhysChem* **2004**, *5*, 252−257.
(4) Klimov, D. K.; Thirumalai, D. *Proc. Natl. Acad. Sci. U.S.A.* **1999**, *96*, 6166−6170.
(5) Hyeon, C.; Dima, R.; Thirumalai, D. *Structure* **2006**, *14*, 1633−1645.
(6) Mickler, M.; Dima, R. I.; Dietz, H.; Hyeon, C.; Thirumalai, D.; Rief, M. *Proc. Natl. Acad. Sci. U.S.A.* **2007**, *104*, 20268−20273.
(7) Hyeon, C.; Onuchic, J. N. *Proc. Natl. Acad. Sci. U.S.A.* **2007**, *104*, 2175−2180.
(8) Tehver, R.; Thirumalai, D. *Structure* **2010**, *18*, 471−481.
(9) Lee, J. Y.; Iverson, T. M.; Dima, R. I. *J. Phys. Chem. B* **2011**, *115*, 186−195.
(10) Duan, L.; Zhmurov, A.; Barsegov, V.; Dima, R. *J. Phys. Chem. B* **2011**, *115*, 10133−10146.
(11) Zhmurov, A.; Brown, A. E.; Litvinov, R. I.; Dima, R. I.; Weisel, J. W.; Barsegov, V. *Structure* **2011**, *19*, 1615−1624.
(12) Zhmurov, A.; Dima, R.; Kholodov, Y.; Barsegov, V. *Proteins* **2010**, *78*, 2984−2999.
(13) Zhmurov, A.; Rybnikov, K.; Kholodov, Y.; Barsegov, V. *J. Phys. Chem. B* **2011**, *115*, 5278−5288.
(14) Gardner, M.; Hunt, A.; Goodson, H.; Odde, D. *Curr. Opin. Cell Biol.* **2008**, *20*, 64−70.

(15) Nogales, E.; Wang, H.-W. *Curr. Opin. Cell Biol.* **2006**, *18*, 179−184.
(16) Mandelkow, E.-M.; Mandelkow, E.; Milligan, R. *J. Cell Biol.* **1991**, *114*, 977−991.
(17) Nogales, E.; Wang, H.-W.; Niederstrasser, H. *Curr. Opin. Struct. Biol.* **2003**, *13*, 256−261.
(18) Erickson, H.; Stoffler, D. *J. Cell Biol.* **1996**, *135*, 5−8.
(19) Roll-Mecak, A.; McNally, F. J. *Curr. Opin. Cell. Biol.* **2010**, *22*, 96−103.
(20) Diaz-Valencia, J.; Morelli, M.; Bailey, M.; Zhang, D.; Sharp, D.; Ross, J. L. *Biophys. J.* **2011**, *100*, 2440−2449.
(21) Moores, C.; Yu, M.; Guo, J.; Beraud, C.; Sakowicz, R.; Milligan, R. *Mol. Cell* **2002**, *9*, 903−909.
(22) Oguchi, Y.; Uchimura, S.; Ohki, T.; Mikhailenko, S. V.; Ishiwata, S. *Nat. Cell Biol.* **2011**, *13*, 846−852.
(23) White, S.; Evans, K.; Lary, J.; Cole, J.; Lauring, B. *J. Cell Biol.* **2007**, *176*, 995−1005.
(24) Gittes, F.; Mickey, B.; Nettleton, J.; Howard, J. *J. Cell Biol.* **1993**, *120*, 923−934.
(25) de Pablo, P.; Schaap, I.; MacKintosh, F.; Schmidt, C. *Phys. Rev. Lett.* **2003**, *91*, 098101−1.
(26) Grafmuller, A.; Voth, G. *Structure* **2011**, *19*, 409−417.
(27) Wells, D.; Aksimentiev, A. *Biophys. J.* **2010**, *99*, 629−637.
(28) Howard, J. *Mechanics of motor proteins and the cytoskeleton*; Sinauer Associates, Inc.: MA, 2001.
(29) Dima, R.; Joshi, H. *Proc. Natl. Acad. Sci.* **2008**, *105*, 15743−15748.
(30) Maier, B.; Potter, L.; So, M.; Seifert, H. S.; Sheetz, M. P. *Proc. Natl. Acad. Sci. U.S.A.* **2002**, *99*, 16012−16017.
(31) Joshi, H.; Momin, F.; Haines, K.; Dima, R. *Biophys. J.* **2010**, *98*, 657−666.
(32) Veitshans, T.; Klimov, D. K.; Thirumalai, D. *Folding Des.* **1996**, *2*, 1−22.
(33) Nogales, E.; Whittaker, M.; Milligan, R.; Downing, K. *Cell* **1999**, *96*, 79−88.
(34) Dietz, H.; Berkemeier, F.; Bertz, M.; Rief, M. *Proc. Natl. Acad. Sci.* **2006**, *103*, 127724−127728.
(35) Schaap, I.; Carrasco, C.; de Pablo, P.; Schmidt, C. *Biophys. J.* **2011**, *100*, 2450−2456.
(36) Kikumoto, M.; Kurachi, M.; Tosa, V.; Tashiro, H. *Biophys. J.* **2006**, *90*, 1687−1696.
(37) Erickson, H.; Taylor, D.; Taylor, K.; Bramhill, D. *Proc. Natl. Acad. Sci.* **1996**, *93*, 519−523.
(38) Sanchez, S. A.; Brunet, J. E.; Jameson, D. M.; Lagos, R.; Monasterio, O. *Protein Sci.* **2004**, *13*, 81−88.
(39) Hartman, J.; Mahr, J.; McNally, K.; Okawa, K.; Iwamatsu, A.; Thomas, S.; Cheesman, S.; Heuser, J.; Vale, R.; McNally, F. *Cell* **1998**, *93*, 277−287.
(40) Rouiller, I.; DeLaBarre, B.; May, A.; Weis, W.; Brunger, A.; Milligan, R.; Wilson-Kubalek, E. *Nat. Struct. Biol.* **2002**, *9*, 950−957.
(41) Roll-Mecak, A.; Vale, R. *Nature* **2008**, *451*, 363−368.
(42) Kravats, A.; Jayasinghe, M.; Stan, G. *Proc. Natl. Acad. Sci.* **2011**, *108*, 2234−2239.
(43) McNally, F.; Vale, R. *Cell* **1993**, *75*, 419−429.
(44) Llorca, O.; Martin-Benito, J.; Ritco-Vonsovici, M.; Grantham, J.; Hynes, G. M.; Willison, K. R.; Carrascosa, J. L.; Valpuesta, J. M. *EMBO J.* **2000**, *19*, 5971−5979.
(45) Ahmad, F.; Yu, W.; McNally, F.; Baas, P. *J. Cell Biol.* **1999**, *145*, 305−315.
(46) SchekIII, H.; Gardner, M.; Cheng, J.; Odde, D.; Hunt, A. *Curr. Biol.* **2007**, *17*, 1445−1455.
(47) Caplow, M.; Shanks, J. *Mol. Biol. Cell* **1996**, *7*, 663−675.
(48) Humphrey, W.; Dalke, A.; Schulten, K. *J. Mol. Graphics* **1996**, *14*, 33−38.